

An investigation of GPU-based stiff chemical kinetics integration methods

Nicholas J. Curtis^{a,*}, Kyle E. Niemeyer^b, Chih-Jen Sung^a

^a*Department of Mechanical Engineering*

University of Connecticut, Storrs, CT 06269, USA

^b*School of Mechanical, Industrial, and Manufacturing Engineering*

Oregon State University, Corvallis, OR 97331, USA

Abstract

A fifth-order implicit Runge–Kutta method and two fourth-order exponential integration methods equipped with Krylov subspace approximations were implemented for the GPU and paired with the analytical chemical kinetic Jacobian software `pyJac`. The performance of each algorithm was evaluated by integrating thermochemical state data sampled from stochastic partially stirred reactor simulations and compared with the commonly used CPU-based implicit integrator `CVODE`. We estimated that the implicit Runge–Kutta method running on a single GPU is equivalent to `CVODE` running on 12–38 CPU cores for integration of a single global integration time step of 10^{-6} s with hydrogen and methane models. In the stiffest case studied—the methane model with a global integration time step of 10^{-4} s—thread divergence and higher memory traffic significantly decreased GPU performance to the equivalent of `CVODE` running on approximately three CPU cores. The exponential integration algorithms performed more slowly than the implicit integrators on both the CPU and GPU. Thread divergence and memory traffic were identified as the main limiters of GPU integrator performance, and techniques to mitigate these issues were discussed. Use of a finite-difference Jacobian on the GPU—in place of the analytical Jacobian provided by `pyJac`—greatly decreased integrator performance due to thread divergence, resulting in maximum slowdowns of $7.11\text{--}240.96\times$; in comparison, the corresponding slowdowns on the CPU were just $1.39\text{--}2.61\times$, underscoring the importance of use of an analytical Jacobian for efficient GPU integration. Finally, future research directions for working towards enabling realistic chemistry in reactive-flow simulations via GPU/SIMD accelerated stiff chemical kinetic integration were identified.

Keywords: Chemical kinetics, Stiff chemistry, Integration algorithms, GPU

*Corresponding author

Email address: nicholas.curtis@uconn.edu (Nicholas J. Curtis)

1. Introduction

The need for accurate chemical kinetic models in predictive reactive-flow simulations has driven the development of detailed oxidation models for hydrocarbon fuels relevant to transportation and energy generation applications. At the same time, growing understanding of hydrocarbon oxidation processes resulted in orders of magnitude increases in model size and complexity. Contemporary detailed chemical kinetic models relevant to jet fuel [1], diesel [2], gasoline [3], and biodiesel [4] surrogates consist of hundreds to thousands of species with potentially tens of thousands of reactions. Furthermore, kinetic models for large hydrocarbon fuels tend to exhibit high chemical stiffness that requires implicit integration algorithms for practical solution. The cost of these algorithms scales at best quadratically—and at worst cubically—with the number of species in a model [5]. Lu and Law [5] extensively reviewed techniques for reducing the cost of using detailed chemical kinetic models. In addition to the methods discussed in their work, significant effort has also been directed towards improvements of the integration algorithms.

Reactive-flow modeling codes commonly rely on high-order implicit integration techniques to solve the stiff governing equations posed by chemical kinetic models. These methods require repeated evaluation and factorization of the chemical kinetic Jacobian matrix to solve the associated nonlinear algebraic equations through iterative solutions of linear systems of equations—the cost of which scales quadratically and cubically, respectively, with the number of species in a model. However, significant cost savings in the Jacobian evaluation can be realized by using an analytical formulation, rather than the typical evaluation via finite difference approximations. This approach eliminates numerous chemical source term evaluations, and for a sparse Jacobian (e.g., formulated in terms of species concentrations) the cost of evaluation can drop to a linear dependence on the number of species in the model [5].

In this work, our efforts to accelerate simulations with chemical kinetics focus on improving the integration strategy itself, via development of new algorithms and using high-performance hardware accelerators such as graphics processing units (GPUs) and similar single-instruction multiple-data (SIMD) devices. Central processing unit (CPU) clock speeds increased regularly over the past few decades—commonly known as Moore’s Law—however, power consumption and heat dissipation issues slowed this trend recently. While multicore parallelism has increased CPU performance, recently SIMD processors gained popularity as a low cost, low power consumption, and massively parallel high-performance computing alternative. GPUs were originally developed for graphics/video processing applications and consist of hundreds to thousands of separate processing units,

compared with the tens of cores found on typical CPUs. The SIMD parallelism model differs from a traditional CPU-based multithreading model, with small per-core memory caches and acceleration resulting from executing the same instruction over multiple data. Subsequently, using the SIMD parallelism model requires extra consideration to accelerate chemical kinetics integration.

This study used the NVIDIA CUDA framework [6, 7], hence the following discussion will use CUDA terminology; however, the concepts within are widely applicable to SIMD processing. The basic parallel function call on a GPU, termed a kernel, is broken up into a grid of thread blocks. A GPU consists of many streaming multiprocessors (SMs), each of which is assigned one or more thread blocks in the grid. The SMs further subdivide the blocks into groups of 32 threads called warps, which form the fundamental CUDA processing entity. The resources available on a SM (memory, cores, registers, etc.) are split between the warps from all the assigned blocks. The threads in a warp are executed in parallel on CUDA cores, with multiple warps typically being executed concurrently on a SM. Thread divergence occurs when the threads in a warp follow different execution paths, e.g., due to if/then branching, and is a key performance concern for SIMD processing. In such cases the divergent execution paths must execute in serial, causing a slowdown. Furthermore, as compared with a typical CPU, GPUs possess relatively small memory caches and few registers per SM. These resources are further split between all the blocks/warps running on that SM. Overuse of these resources can cause slow global memory accesses for data not stored locally in-cache or can even reduce the number of blocks assigned to each SM. The performance tradeoffs of various CUDA execution patterns are quite involved and beyond the scope of this work; for more details we refer the interested reader to several works that discussed these topics in depth [8–10]. Instead, we will briefly highlight key considerations for CUDA-based chemical kinetic ordinary differential equation (ODE) integration.

The extent of thread cooperation within a CUDA-based chemical kinetic ODE integration algorithm is a key point that shapes much of implementation. GPU-accelerated chemical kinetic solvers typically follow either a “per-thread” pattern [11–13], in which each individual GPU thread solves a single set of chemical kinetic ODEs, or a “per-block” approach [12, 14], in which all the threads in a block cooperate to solve a single set of chemical kinetic ODEs. The greatest potential benefit of a per-thread approach is that a much larger number of ODEs can theoretically be solved concurrently; the number of blocks that can be executed concurrently on each SM is usually around eight, whereas typical CUDA launch configurations in this work consist of 64 threads per block, or 512 sets of ODEs solved concurrently per SM. Unfortunately, the larger amount of parallelism

offered by a per-thread approach does not come without drawbacks. A per-thread approach may encounter more cache-misses, since the memory available per SM must now be split between many more sets of ODEs. This results in expensive global memory loads. The performance of a per-thread approach can also be greatly impacted by thread divergence, because different threads may follow different execution paths within the ODE integration algorithm itself [12, 13]. For this reason, implicit integration algorithms—which typically have complex branching and evaluation paths—may suffer more from thread divergence when implemented on a per-thread basis than relatively simpler explicit integration techniques [12]. The impact of thread divergence on integrators is typically less severe when following a per-block strategy, since the execution path of each thread is planned by design of the algorithm. A per-block approach also offers significantly more local cache memory and available registers for solving a set of ODEs, and thus memory access speed and cache size are less of a concern. However, in our experience, optimizing use of these resources requires significant manual tuning and makes it more difficult to generalize the developed algorithm between different chemical kinetic models—a key feature for potential non-academic applications. In addition, Stone and Davis [12] showed that a per-thread implicit integration algorithm outperforms the per-block implementation of the same algorithm in the best-case scenario (elimination of thread divergence by choice of identical initial conditions).

Various studies in recent years explored the use of high-performance SIMD devices to accelerate (turbulent) reactive-flow simulations. Spafford et al. [15] investigated GPUs for accelerating a direct numerical simulation code for turbulent combustion, demonstrating a sub-order of magnitude speedup in evaluating the species production rates on the GPU, as compared with a highly optimized message-passing-interface-based CPU code. Shi et al. [16] used a GPU to evaluate species rates and factorize the Jacobian for the integration of (single) independent kinetics systems, showing order-of-magnitude or greater speedups for large kinetic models over a CPU-based code which utilized standard CHEMKIN [17] and LAPACK [18] libraries for the same operations. Niemeyer et al. [11] implemented an explicit fourth-order Runge–Kutta integrator for the GPU, and found a speedup of nearly two orders of magnitude with a nonstiff hydrogen model when compared with the CPU counterpart. In a related work, Shi et al. [19] developed a GPU-based stabilized explicit solver and paired it with a CPU-based implicit solver that handled integration of the most-stiff chemistry cells in a three-dimensional premixed diesel engine simulation, demonstrating an overall speedup of two to three times. Le et al. [20] implemented GPU versions of two high-order shock-capturing reactive-flow codes, and found a 30–50 \times speedup over the baseline single-core CPU version. Stone and Davis [12]

implemented the implicit VODE [21] solver for the GPU and achieved an order of magnitude speedup over the baseline CPU version. They also showed that GPU-based VODE exhibits significant thread divergence, as expected due to its complicated program flow compared with an explicit integration scheme. Furthermore, Stone and Davis [12] found that a per-thread implementation outperforms a per-block version of the same algorithm for $\sim 10^4$ independent ODEs or more; the per-block implementation reached its maximum speedup for a smaller number of ODEs ($\sim 10^3$). Niemeyer and Sung [13] demonstrated an order-of-magnitude speedup for a GPU implementation of a stabilized explicit second-order Runge–Kutta–Chebyshev algorithm over a multicore CPU implementation of VODE for moderately stiff chemical kinetics. They also investigated levels of thread divergence due to differing integrator time-step sizes, and found that it negatively impacts overall performance for dissimilar ODE initial conditions in a thread-block. Sewerin and Rigopoulos [14] implemented a three-stage/fifth-order implicit Runge–Kutta GPU method [22] on a per-block basis, and found a $1.8\times$ slowdown at best compared with the same on an eight-core CPU.

While increasing numbers of studies have explored GPU-based chemical kinetics integration, there remains a clear need to find or develop integration algorithms simultaneously suited for the SIMD parallelism of GPUs (along with similar accelerators) and capable of handling stiffness. In this work we will investigate GPU implementations of several explicit and implicit integration techniques, as compared with their CPU counterparts and the baseline CPU CVODE [23] algorithm. Several groups [24, 25] previously suggested so-called matrix-free methods as potential improvements to the expensive linear-system solver required in standard implicit methods. These methods do not require direct factorization of the Jacobian, but instead use an iterative process to approximate the action of the factorized Jacobian on a vector. Furthermore, Hochbruck and Lubich [26] demonstrated that the action of the matrix exponential on a vector obtained using Krylov subspace approximation converges faster than corresponding Krylov methods for the solution of linear equations. Others explored these explicit exponential methods for applications in stiff chemical systems [27, 28] and found them stable for time-step sizes greatly exceeding the typical explicit stability bounds. The explicit nature of these algorithms makes them potentially better suited for SIMD acceleration due to an expected reduction of thread divergence (for a per-thread implementation) compared with implicit methods. Since this premise has not been demonstrated in the literature, we aim to conduct a systematic investigation to test and compare their performance. Finally, we will study the three-stage/fifth-order implicit Runge–Kutta algorithm [22] investigated by Sewerin and Rigopoulos [14] here to determine the impact of increasing chemical stiffness on the algorithm and the performance

benefits of using an analytical Jacobian matrix, such as that developed by Niemeyer et al. [29–31].

The rest of the paper is structured as follows. Section 2 lays out the methods and implementation details of the algorithms used here. Subsequently, Sec. 3 presents and discusses the performance of the algorithms run using a database of partially stirred reactor thermochemical states, with particular focus on the effects of thread divergence and memory traffic. Further, this work is a starting point to reduce the cost of reactive-flow simulations with realistic chemistry via SIMD-accelerated chemical kinetic evaluation. Thus, we explore the potential impact of current state-of-the-art GPU-accelerated stiff chemical kinetic evaluation on large-scale reactive-flow simulations in Sec. 3, while identifying the most promising future directions for GPU/SIMD accelerated chemical kinetic integration in Sec. 4. Finally, Appendix A and Appendix B present supplementary data including L^AT_EX source files, validation and performance data, plotting scripts, and unscaled plots of integrator runtimes.

2. Methodology

In this section, we discuss details of the algorithms implemented for the GPU along with third-party software used. The generation of testing conditions will be discussed briefly, and the developed solvers will be verified for expected order of error.

2.1. Integration techniques

We investigated GPU implementations of three integration methods in this work, comparing them against equivalent CPU versions and a CPU-only implicit algorithm. While we describe important details or changes made in this work, full descriptions of all algorithms may be found in the cited sources. The pyJac software [29–31] provided subroutines for both chemical source terms and the analytical Jacobian matrix used by CPU- and GPU-based algorithms. We evaluated the relative performance impact of using a finite-difference Jacobian matrix (as compared with an analytical Jacobian) for both platforms with a first-order finite difference method based on that of CVODE [23]. pyJac also provided the chemical source terms used by the finite-difference Jacobian in all cases. We direct readers to our previous work [30, 31] for verification and performance assessments of pyJac itself.

First, the CVODE solver [23, 32] (part of the SUNDIALS suite [33]) provided the baseline performance of a typical CPU-based (maximum of fifth-order) implicit integration technique. In addition, we developed CPU versions of the methods under investigation for direct comparison to

the high-order implicit technique. These include the three-stage/fifth-order implicit Runge–Kutta algorithm [22] (**Radau-IIA**), the fourth-order exponential Rosenbrock-like method of Hochbruck et al. [34] (**exp4**), and the newer fourth-order exponential Rosenbrock method [35] (**exprb43**). For the exponential methods, we used the method of rational approximants [36] paired with the Carathéodory–Fejér method [37, 38] to approximate the action of the matrix exponential on a vector, as suggested by Bisetti [27]. This technique relied on the external FFTW3 library [39, 40]. However, unlike the approach of Bisetti [27], we developed a custom routine based on the algorithm presented by Stewart [41] to perform LU decomposition of the Hessenberg matrix resulting from the Arnoldi iteration. Convergence of the Arnoldi iteration algorithm was computed using the second term of the exponential matrix/vector product infinite series, as suggested in several works [27, 42]. The exponential integrators used a rational approximant of type (10, 10) as suggested by Bisetti [27]. To ensure high performance of CPU-based methods, the Intel MKL library version 11.3.2 handled linear algebra (i.e., BLAS/LAPACK) operations. Next, we developed GPU versions of the **Radau-IIA**, **exp4**, and **exprb43** methods. These follow the same descriptions as the CPU versions, but require specialized implementations of several BLAS and LAPACK methods, mostly related to LU factorization of the Jacobian or Hessenberg matrices. All GPU routines were developed using the NVIDIA CUDA framework [6, 7]. All solvers used adaptive time-stepping techniques; the **Radau-IIA** and **CVODE** integrators have built-in adaptive time-stepping, while the exponential methods used a standard adaptive time-stepping technique [22]. Finally, the adaptive time stepping procedures of all integrators used absolute and relative tolerances of 10^{-10} and 10^{-6} , respectively, throughout the work.

2.2. Testing conditions

In order to measure the performance of the integrators for realistic conditions, a database of thermochemical states covering a wide range of temperatures and species mass fractions was generated using a previously developed constant-pressure stochastic partially stirred reactor (PaSR) code [29, 31]. We selected two chemical kinetic models to span the range of model sizes typically used in high-fidelity simulations: the hydrogen model of Burke et al. [43] with 13 species and 27 reactions, and the GRI-Mech 3.0 model for methane with 53 species and 325 reactions [44]. The PaSR simulations were performed at the conditions listed in Table 1 for 10 residence times to reach a statistical steady state; Niemeyer et al. [31] describe the PaSR simulation process in greater detail, which follows approaches used by others [45–47]. The PaSR particles were initialized using

the equilibrium state, and gradually move away from equilibrium conditions due to mixing, inflow, and outflow. In order to reduce the influence of equilibrium conditions on the solution runtime trends for small numbers of ODEs, the first 1000 datapoints were removed from each database; this corresponds to a single pairing time, τ_{pair} , the time interval at which selected particles in the reactor are randomly swapped with inflowing particles. At this point in the simulation, $\sim 80\%$ of the particles were at or near an equilibrium state, and by the 5000th datapoint only $\sim 20\%$ of the particles were near equilibrium. The hydrogen and GRI-Mech 3.0 databases consisted of 899,900 and 449,900 total conditions, respectively.

Parameter	H ₂ /air	CH ₄ /air
ϕ	1.0	
T_{in}	400, 600, and 800 K	
p	1, 10, and 25 atm	
N_p	100	
τ_{res}	10 ms	5 ms
τ_{mix}	1 ms	1 ms
τ_{pair}	1 ms	1 ms

Table 1: PaSR parameters used for hydrogen/air and methane/air premixed combustion cases, where ϕ indicates equivalence ratio, T_{in} is the temperature of the inflowing particles, p is the pressure, N_p is the number of particles in the reactor, τ_{res} is the residence time, τ_{mix} is the mixing time, and τ_{pair} is the pairing time.

2.3. Solver verification

To investigate the correctness of the developed solvers, the first 10,000 conditions in the hydrogen database were integrated by each solver using a global time-step size of 10^{-6} s. The error for condition i was then determined using the weighted root-mean-square error

$$E_i(t) = \left\| \frac{y_i(t) - \hat{y}_i(t)}{\text{atol} + \hat{y}_i(t) \times \text{rtol}} \right\|_2, \quad (1)$$

where the $y_i(t)$ is the solution obtained from the various solvers, atol/rtol are the absolute/relative tolerances, and $\hat{y}_i(t)$ is the “true” solution obtained via **CVODE** using an internal time-step of $\delta t = 10^{-10}$ s and absolute/relative tolerances of 10^{-20} and 10^{-15} , respectively; note that the more stringent tolerances were used only to obtain the “true” solution. The maximum error over all conditions:

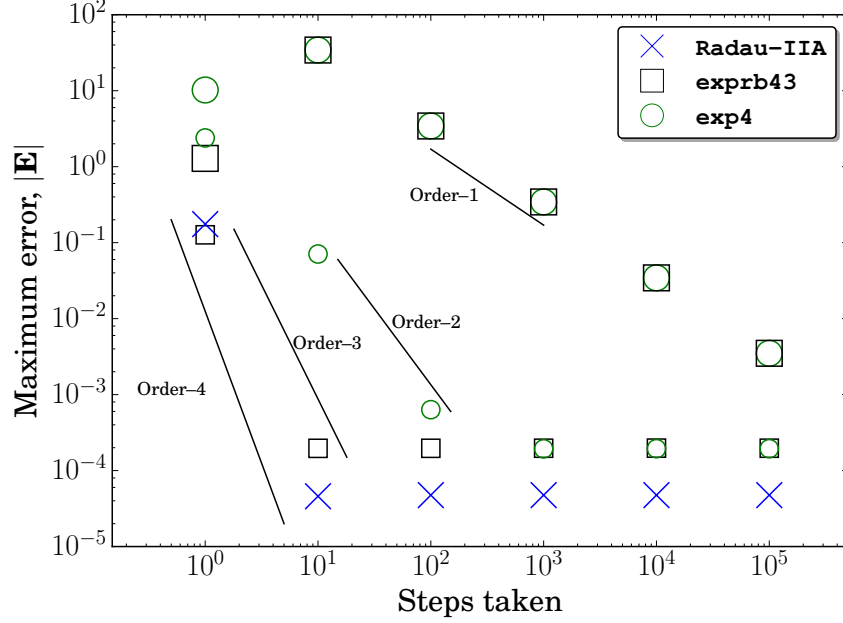


Figure 1: Maximum error of the various CPU solvers as a function of the total number of internal integration steps taken (corresponding to decreasing time-step size). Larger square and circle symbols indicate the use of Krylov subspace approximations with the exponential methods, while the smaller symbols indicate the use of “exact” Krylov subspaces.

$$|\mathbf{E}| = \max_{i=1,\dots,10,000} \{E_i(t)\} \quad (2)$$

was then used to measure the error of each solver. The error measurement used the same tolerances as for the performance testing ($\text{atol} = 10^{-10}$ and $\text{rtol} = 10^{-6}$, respectively). The constant internal time-step size was then varied from 10^{-6} – 10^{-11} s—corresponding to 10^0 – 10^5 internal integration steps—to measure the convergence rates of the various solvers.

Figure 1 shows the convergence of error for the CPU solvers with decreasing internal time-step size, shown as increasing number of integration steps taken. The error of the Radau-IIA integrator drops nearly four orders of magnitude when changing from a single internal time step of 10^{-6} s to ten internal time steps of 10^{-7} s each, i.e., fourth-order convergence. Increasing the number of integration steps—by further reducing the internal time-step size—past this point does not reduce error further, due to numerical precision effects; this likely causes the apparent order reduction of the Radau-IIA solver, which is nominally fifth order. The exponential solvers utilizing an approximate Krylov subspace exhibit larger levels of error in general, with $|\mathbf{E}| \sim \mathcal{O}(1)$ – $\mathcal{O}(10)$ for a single

internal integration step of $\delta t = 10^{-6}$ s. As the time-step size is decreased, the convergence of the Arnoldi algorithm is affected by the internal integration time-step size (the matrix exponentials and error estimates are scaled by the internal time-step). To study the effect of the Arnoldi algorithm on error, Fig. 1 also presents the error convergence of the exponential integrators with the Krylov approximation error reduced far below the error of the overall method. Practically, this was accomplished by detecting when the n th Krylov subspace vector approaches zero, a condition known as the “happy breakdown” in literature [48]. At this limit, the approximate exponential matrix/vector product approaches the exact value and thus the Krylov approximation induces negligible error. Figure 1 shows that the exponential methods achieve only first-order convergence to the true solution with the approximate Krylov subspace, but both methods converge at higher rates with the “exact” Krylov subspace. The nominal fourth-order convergence of the `exp4` algorithm is a classical nonstiff order, and thus order reduction is expected for stiff problems [27, 49]; the `exp4` solver reaches roughly second-order convergence with the “exact” Krylov subspace. The `exp43` solver reaches third-order convergence with the “exact” Krylov subspace—again, likely due to numerical precision effects, since further reduction of the internal time-step size does not affect error. Furthermore, the error of Krylov subspace approximation dominates the error measurement $|\mathbf{E}|$. From Fig. 1 we conclude that all solvers produce reasonably accurate solutions as compared with CVODE. Additionally, although not shown, the GPU solvers produce identical results.

3. Results and discussion

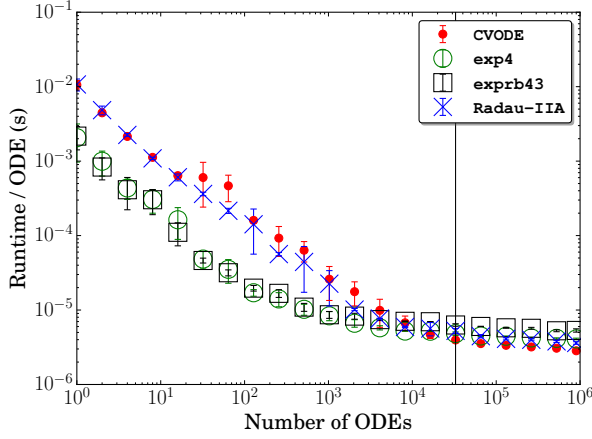
We studied the performance of the three integrators by testing each on the PaSR conditions described in Sec. 2.2 for two different global integration time-step sizes: $\Delta t = 10^{-6}$ s and $\Delta t = 10^{-4}$ s. Using a larger global time step induces additional stiffness and allows evaluation of the performance of the developed solvers on the same chemical kinetic model with varying levels of stiffness. In reactive-flow simulations, the chemical integration time-step is typically determined by the flow time-scale and stability requirements determined by the Courant–Friedrichs–Lewy number; typical time-step values range from 10^{-6} – 10^{-1} s [50]. Although the time-step size used in a given simulation depends highly on the problem and numerical methods, large-eddy simulations usually require higher time resolution than Reynolds-averaged Navier–Stokes simulations [51]. Hence, the time-steps chosen for study are representative of realistic values used in large-eddy [52, 53] and Reynolds-averaged Navier–Stokes [54, 55] simulations. Runtimes are reported as the average over five runs, where each run started from the same set of PaSR conditions. All CPU integrators were compiled using `gcc`

4.8.5 (with the compiler options “-O3 -funroll-loops -mtune=native”) and executed in parallel via OpenMP on four ten-core 2.2 GHz Intel Xeon E5-4640 v2 CPUs with 20 MB of L3 cache memory. OpenMP was used to parallelize on a per-condition basis; i.e., each individual OpenMP thread was responsible for integrating a single set of chemical kinetic ODEs, rather than cooperating with other OpenMP threads to solve the same. A six-core 2.67 GHz Intel Xeon X5650 CPU hosted the GPU integrators, which were compiled using `nvcc` 7.5.17 (with compiler options “-arch=sm_20 -O3 -maxrregcount 63 --ftz=false --prec-div=true --prec-sqrt=true --fmad=false”) and run on a single NVIDIA Tesla C2075 with 6 GB of global memory. Reported runtimes for the GPU-based algorithms include time needed for CPU–GPU data transfer before and after each global time step; in addition, the function `cudaSetDevice()` initialized the GPU before timing to avoid any device initialization delay. The open-source `pyJac` software [29–31] produced CPU and GPU custom source-code functions for the chemical source terms and analytical Jacobian matrix evaluation. Finally, the L1/shared-memory cache was set to prefer a larger L1 cache using the `cudaDeviceSetCacheConfig()` function.

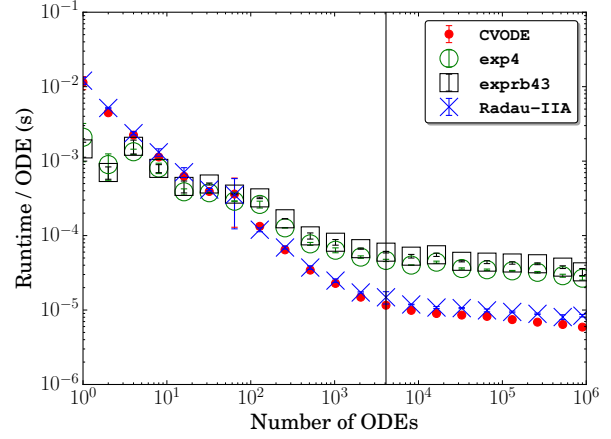
3.1. Runtime performance

For all cases in this section, the integrator runtimes are presented as the runtime per ODE solved, for two reasons. First, saturation of the available computational resources becomes visually apparent (transition from a nearly linear decrease to a flat trend), and second, it allows certain other performance trends (e.g., the effects of thread divergence) to be easily highlighted. The presentation of the performance data in raw form is also available in [Appendix B](#) for completeness.

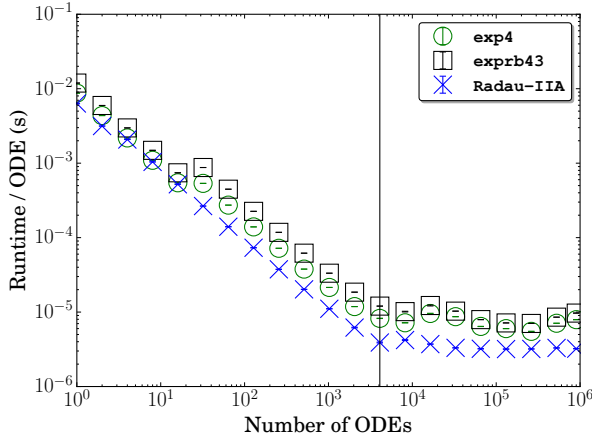
Figure 2 shows the runtimes of the CPU and GPU integrators for the hydrogen model. In Fig. 2a the runtimes per ODE for the CPU integrators for a single global time-step of $\Delta t = 10^{-6}$ s decrease approximately linearly with the number of ODEs for small numbers of initial conditions (shown here on a log-log plot). For small numbers of ODEs, the exponential integrators are faster than the implicit integration techniques due to the modest stiffness of the hydrogen model; even with many near-equilibrium states removed from the beginning of the PaSR database, the model is not particularly stiff for this small time-step size. Larger numbers of ODEs begin to saturate the CPU resources, and the runtime per ODE levels off to a more constant value. Eventually, relatively more stiff conditions are encountered and the performance of the implicit integration techniques catches up and then surpasses that of the exponential integrators; `CVODE` is the most efficient solver on the CPU when solving more than 10^4 ODEs; however, `CVODE` is only $\sim 1.87\times$ faster than the



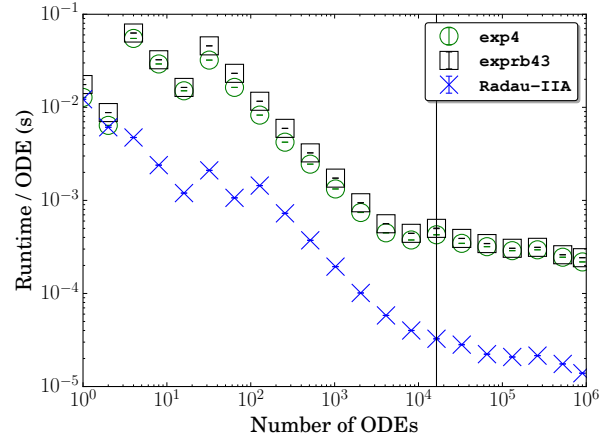
(a) CPU performance results for $\Delta t = 10^{-6}$ s



(b) CPU performance results for $\Delta t = 10^{-4}$ s



(c) GPU performance results for $\Delta t = 10^{-6}$ s



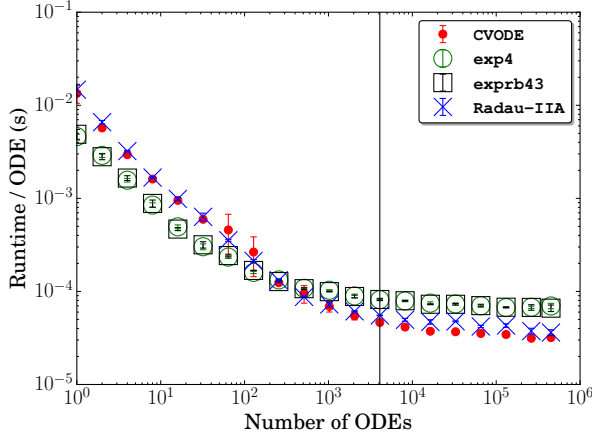
(d) GPU performance results for $\Delta t = 10^{-4}$ s

Figure 2: Average runtimes of the integrators on the CPU and GPU, scaled by the number of ODEs, for the hydrogen model at two different global time-step sizes. Estimation of where the runtime per ODE reaches a constant value (based on the results for CVODE/Radau-IIA for the CPU/GPU respectively) is marked in with a vertical line for all cases. Error bars indicate standard deviation.

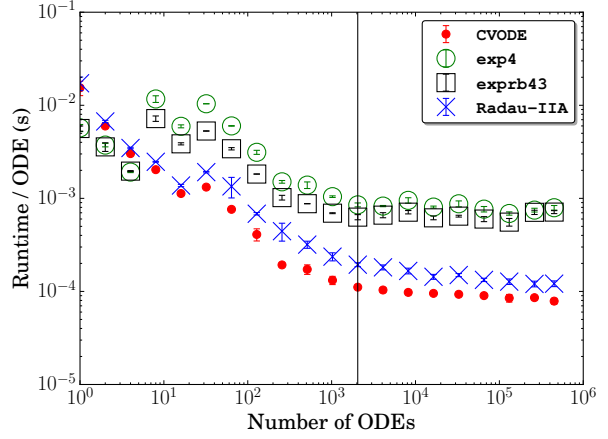
slowest solver (`exprb43`) on the whole database. Figure 2c shows the performances of the GPU integrators for the smaller global time-step size, which exhibit similar trends as the CPU solvers: a linearly decreasing solution cost that reaches a roughly constant value beyond 10^3 – 10^4 ODEs. Unlike for the CPU solvers, the GPU-based `Radau-IIA` performs faster than the exponential solvers for all numbers of ODEs. As will be seen in Sec. 3.3, both solver classes experience minimal thread divergence due to differing internal integration time-step size in this case. Therefore, we conclude that the relatively slower runtimes per ODE for the exponential algorithms on the GPU results from thread divergence in the Arnoldi iteration—caused by varying Krylov subspace sizes between threads.

Figures 2b and 2d show the performance of the integration algorithms on both platforms for the hydrogen model with a single larger global time step ($\Delta t = 10^{-4}$ s). The performances of the CPU integration algorithms show similar trends to those of the smaller time-step size case: decreasing cost per ODE before reaching a more constant performance for higher numbers of ODEs. The larger time-step size induces additional stiffness, and the implicit solvers are more efficient for most numbers of ODEs; `CVODE` is again the most efficient CPU solver. Figure 2d shows the performance of the GPU solvers for the larger global time-step size. The exponential solvers exhibit significant spikes in computational cost when changing from 2–4 and 16–32 ODEs, with the latter mimicked somewhat by the implicit `Radau-IIA` solver. A jump in solution cost between 2–4 ODEs is also present for the CPU exponential integrators, indicating chemical stiffness as the primary cause. On the other hand, between 16–32 ODEs the CPU exponential solvers exhibit only a very minor performance decrease, while the GPU-based `Radau-IIA` also shows a decrease in performance at the same point—a trend completely absent in the CPU `Radau-IIA` version. These factors indicate that thread divergence also plays a key role in the performance trend here, and will be investigated further in Sec. 3.3. As in case of the smaller global time-step size, the `Radua-IIA` solver is the most efficient GPU algorithm in all cases.

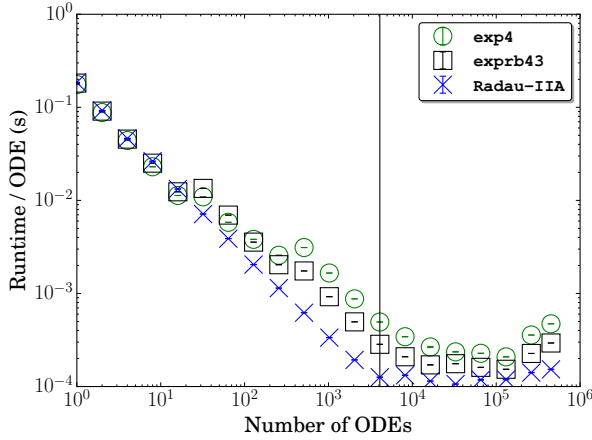
Figure 3 shows the runtime of the integrators for the GRI-Mech 3.0 model. Similar to the hydrogen case for the smaller global time-step size, the CPU exponential integrators are more efficient (Fig. 3a) for the near-equilibrium conditions at the beginning of the database. For larger numbers of conditions, the implicit integrators are more efficient, and `CVODE` again performs the fastest. Compared with the hydrogen model (Fig. 2a), the `CVODE` performs better than the exponential algorithms for the GRI-Mech 3.0 model with the small global time-step size (Fig. 3a), reaching a speedup of $2.18 \times$ over `exp4` on the whole database; this results from the higher stiffness



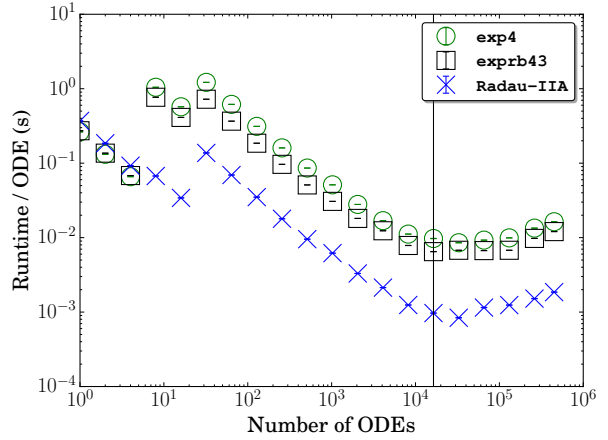
(a) CPU performance results for $\Delta t = 10^{-6} \text{ s}$



(b) CPU performance results for $\Delta t = 10^{-4} \text{ s}$



(c) GPU performance results for $\Delta t = 10^{-6} \text{ s}$



(d) GPU performance results for $\Delta t = 10^{-4} \text{ s}$

Figure 3: Average runtimes of the integrators, scaled by number of ODEs, on the CPU and GPU for the GRI-Mech 3.0 model at two different global time-step sizes. Estimation of where the runtime per ODE reaches a constant value (based on the results for CVODE/Radau-IIA for the CPU/GPU respectively) is marked in with a vertical line for all cases. Error bars indicate standard deviation.

present in the model. This performance gap between the CPU implicit/exponential integrators increases for the larger global time-step size (Fig. 3b); **CVODE** is $10.1 \times$ faster than **exp4** on the whole database. Comparing the performance of the CPU implicit solvers between the two kinetic models shows roughly an order-of-magnitude performance decrease for both global time-step sizes. This phenomena, due largely to the increase in model size, is also seen for the **Radau-IIA** GPU solver for the smaller global time-step size; the performance of which decreases by just over an order of magnitude. However, for the larger global time-step size, the GPU-based **Radau-IIA** solver performs roughly two orders-of-magnitude slower compared with the hydrogen case. As will be examined in Sec. 3.3, this dramatic decrease likely results from increased thread divergence in the **Radau-IIA** solver, as well as the increased memory traffic inherent in the larger model.

Unlike for the hydrogen model, the **exprb43** solver outperforms **exp4** with the GRI-Mech 3.0 model in almost all cases for the larger global time-step size for both the CPU and GPU. Although the **exprb43** and **exp4** algorithms each require three exponential matrix function approximations per step, a single internal time step of **exprb43** is more expensive due to the extra chemical source term evaluations, matrix multiplications, and higher-order exponential matrix function requirement. As such, the relatively simpler CPU **exp4** integrator outperforms the CPU **exprb43** integrator for the hydrogen model where there is relatively less chemical stiffness. However, as previously discussed the **exp4** algorithm may experience order reduction for stiff problems, and the **exprb43** algorithm typically outperforms **exp4** on both the CPU and GPU in the larger global time-step GRI-Mech 3.0 case as a result.

3.2. CPU/GPU performance comparison

Comparing the performance of CPU- and GPU-based integrators in a meaningful way is challenging. First, the vastly different nature of the processing cores in each platform eliminates the possibility of comparing performance normalized by core count. In addition, the floating-point operation count is not readily available for chemical kinetic integration—unlike many GPU-accelerated applications where the number of operations required to solve the problem is known, e.g., as in linear-algebra operations or fast Fourier transforms—which precludes comparing performance on the basis of floating-point operations per second (FLOPS). Although the runtimes of the GPU integration algorithms can be directly compared with that of the CPU-based solvers (and often are), these figures do not provide much useful information. For instance, if a GPU algorithm performs $10 \times$ faster than its equivalent on two six-core CPUs, how does this compare to two eight-core CPUs,

etc.?

For researchers in numerical combustion, two issues stand out as particularly important for performance evaluation: runtime and cost. As established in Sec. 1, large-scale reactive-flow simulations with realistic chemical kinetic models are extremely computationally expensive, and remain outside of the capabilities of most in the field. With this in mind, we ask, for a given simulation, what is the effect on the overall runtime of adding more CPU cores compared with adding GPU accelerators? In addition, if a budget is allocated to expand available computational resources, how might these funds be best allocated? To answer these questions, we derived an estimate of the number of CPU cores required for equivalent performance on the GPU.

A nominal performance metric for both the CPU- and GPU-based integration algorithms must first be obtained. As the most efficient solvers in all cases with large numbers of ODEs are **CVODE** for the CPU and **Radau-IIA** for the GPU, these algorithms will be considered the performance benchmarks. Furthermore, most large-scale simulations consist of millions of cells (or more), and therefore we only consider the performance limit of each algorithm (i.e., the cost per ODE of each algorithm in the region where this cost reaches an approximately constant value). To this end, Figs. 2 and 3 show vertical lines where the relative change in runtime per ODE between successive data-points is first smaller than 15% (based on **CVODE**/**Radau-IIA** for the CPU/GPU accordingly). The cost per ODE above and including these thresholds was averaged and forms our nominal performance measure. The CPU performance measure must also be normalized by the total number of cores used: 40. Table 2 presents the ratios of these performance measures, which give estimates for the number of CPU cores required to equal the GPU performance for the cases studied. The GPU is roughly equivalent to 12 or more CPU cores for all cases except GRI-Mech 3.0 with the larger global time-step size, and equivalent to at most 38 cores for the hydrogen case with the smaller global time-step size. With the increasing size of the chemical kinetic model, the equivalent CPU core count of the GPU **Radau-IIA** solver drops significantly. As will be discussed in Sec. 3.3, this drop in performance is primarily due to higher memory traffic requirements, however increased levels of thread divergence also play a role. Although this work represents the current state-of-the-art for implicit integration of stiff chemical kinetic ODEs on the GPU, it is clear that more effort is required to improve GPU performance for larger chemical kinetic models. Approaches to mitigate these issues will be discussed in the subsequent section.

At the time of writing, the ten-core Intel Xeon E5-4640 v2 CPU used in this study was listed for a recommended customer price of \$2725 [56], while a new Tesla C2075 GPU is available for

Global time-step size	# equivalent CPU cores	
	Hydrogen	GRI-Mech 3.0
10^{-6} s	38	12
10^{-4} s	15	3

Table 2: The number of CPU cores (roughly) required for equivalent performance to a single GPU for the combinations of chemical kinetic models and global time-step sizes studied.

~\$1400 [57]. These prices are only rough estimates of the actual cost of these devices, since the actual price for the Intel CPU may be significantly less in a configured server node, while the Tesla C2075 is no longer sold directly by NVIDIA—thus the prices are variable. Furthermore, the performance decrease using an older, cheaper CPU (e.g., the Intel Xeon X5650 used as host processor for the GPU simulations in this work) may not be that large. However, combined with the equivalent core counts in Table 2, this information suggests that the Tesla C2075 is a reasonable investment to supplement computing power for chemical-kinetic integration in large-eddy simulations.

3.3. Effects of thread divergence and memory traffic

Thread divergence and memory traffic are two performance concerns particularly important for chemical kinetic integration on GPU and SIMD platforms. Slowdown due to memory traffic for a GPU integration algorithm implemented on a per-thread basis primarily results from the small amount of on-chip memory available. Implicit integration algorithms, which typically require storage of the Jacobian matrix and/or factorized forms thereof, can quickly overwhelm the registers and L1 cache memory available to each thread and cause many slow global memory accesses. Reformulating the chemical kinetic equations to generate sparse Jacobian matrices [58] would greatly benefit GPU-based integration algorithms due to the reduced memory requirements, and in addition enable use of sparse multiplication/factorization algorithms (from which a CPU-based algorithm would also benefit); this is a planned improvement to the `pyJac` software [29, 31]. Further, the Tesla C2075 GPU used in this study was originally released nearly five years ago and is several generations old; the newer Tesla K40 is available for a similar price, \$2950 [59], as the Xeon E5-4640 v2 CPU used in this study, and has $2\times$ registers available per block [7] and $6.4\times$ as many CUDA cores [60] as the Tesla C2075 used. Using a newer GPU model could significantly improve solver performance for larger models by relieving the scarcity of on-chip memory in a per-thread approach. Finally, a

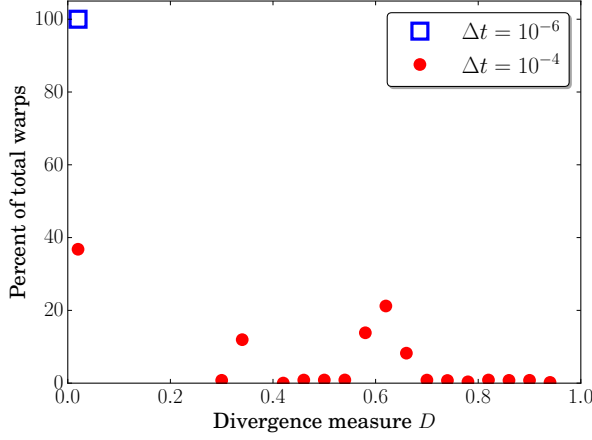
per-block approach may be required to efficiently integrate the largest models on the GPU, due to the much higher amount of cache memory allocated for each ODE solution.

The performance penalty due to thread divergence depends both on the cost of the divergent branches as well as the proportion of the warp that executes each branch. For example, if only one thread in a warp executes an expensive branch (e.g., a Jacobian update) the rest of the warp remains idle during that time, and the SM may become severely underutilized. To investigate the effects of thread divergence further, we adopted a modified version of the quantification of thread divergence of Niemeyer and Sung [13]:

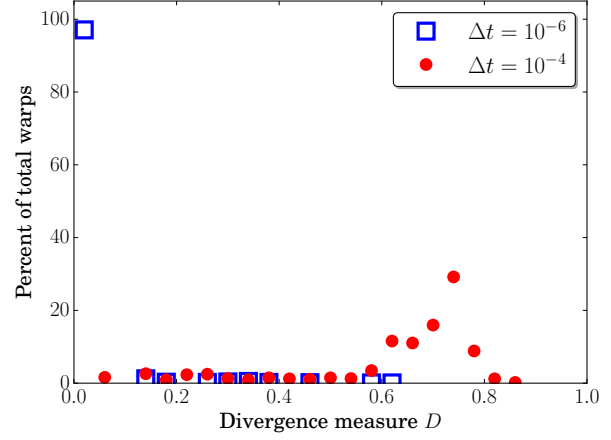
$$D = 1 - \frac{\sum_{i=1}^{32} d_i}{32 \times \max_{i=1, \dots, 32} d_i}, \quad (3)$$

where d_i is the number of internal integrator time steps taken to reach the global time step by thread i in a warp (which consists of 32 threads). D represents the similarity of internal time step counts across threads in a warp—a significant source of thread divergence. If all threads in a warp use identical internal integration time steps and thus the warp experiences no thread divergence from this source, then $D = 0$; however, if a warp experiences an unbalanced number of internal integration time steps, then $D \rightarrow 1$. Differing internal time-step sizes are not the only source of thread divergence for the GPU integration algorithms. For instance, threads in a warp may use different Krylov subspace sizes for the exponential integrators or different numbers of Newton iterations for the **Radau-IIA** solver. Indeed, Sec. 3.1 notes that we suspect thread divergence from differing Krylov subspace sizes as the reason the exponential solvers are less efficient for small numbers of ODEs for the hydrogen model with the small global time-step size. However, these operations clearly cost less than an entire internal integration step (in which they are embedded) and thus we look only at the thread divergence of internal integration time steps. Thread divergence of such operations within an internal integration step could play an important role and will be investigated in our future work.

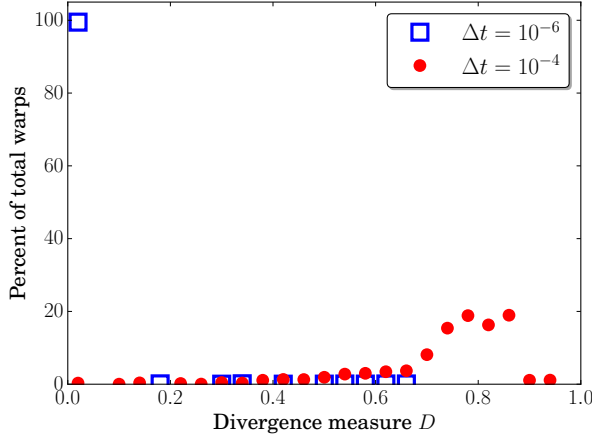
Figures 4a and 4b show the distribution of the divergence measure D for the **Radau-IIA** solver with both global time-step sizes and kinetic models when run on 262,144 ODEs, spread across 8192 warps. For both kinetic models with the smaller global time-step size, nearly 100% of the warps had a divergence measure near zero. Increasing the global time-step size causes the number of warps with high levels of thread divergence (e.g. $D > 0.5$) to increase for both models. For the hydrogen model, over 40% of warps were between $D = 0.55$ and $D = 0.65$, and the approximate equivalent CPU core-count (Table 2) dropped by $2.5 \times$ between the small and large global time-step



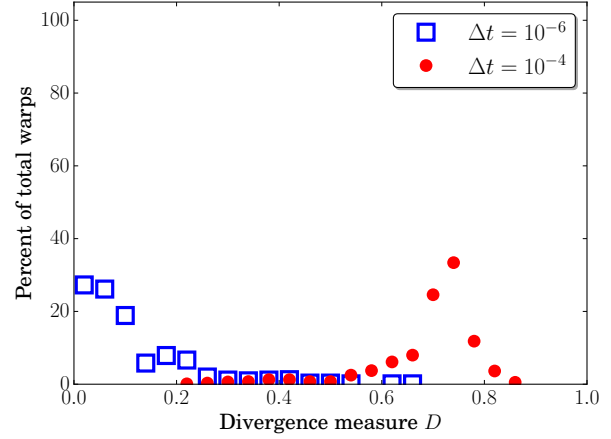
(a) Radau-IIA solver for hydrogen model



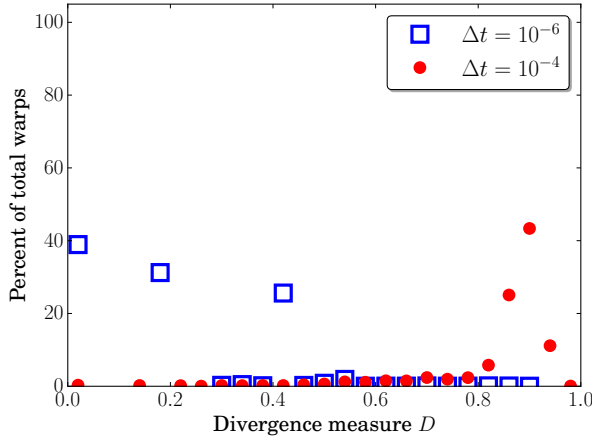
(b) Radau-IIA solver for GRI-Mech 3.0 model



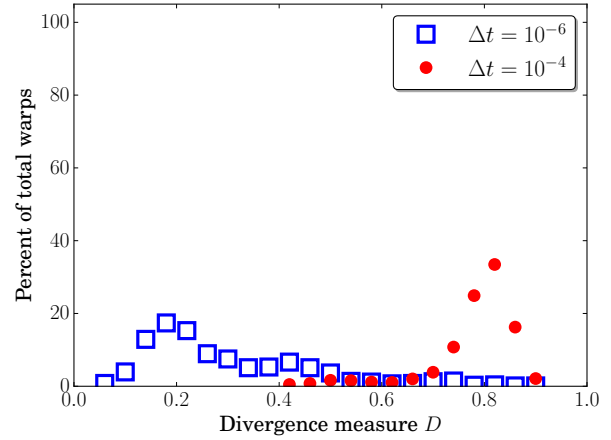
(c) `exp43` solver for hydrogen model



(d) `exp43` solver GRI-Mech 3.0 model



(e) `exp4` solver hydrogen model



(f) `exp4` solver GRI-Mech 3.0 model

Figure 4: Thread divergence estimate for the various solvers for both models and global time-step sizes.

sizes. Further, over 75 % of warps were between $D = 0.6$ and $D = 0.8$ for the GRI-Mech 3.0 model for the larger global time-step size, and subsequently a higher drop in performance of $4\times$ occurred. This observation motivates future work aimed at developing strategies to reduce thread divergence. Potential solutions include adopting an ODE per-block approach [12], reordering ODEs to increase similarity of stiffness inside a warp, or synchronizing internal time-step sizes between threads in a warp. However, Figs. 4a and 4b do not explain the drop in equivalent core count between the hydrogen model and the GRI-Mech 3.0 model for the smaller global time-step size. The minimal thread divergence of the **Radau-IIA** solver for both models at the smaller global time-step size suggests that this drop in performance is primarily caused by the increased memory traffic of the larger model, as well potential thread divergence inside the internal integration step; this further motivates development of a sparse version of the **pyJac** [29, 31] software.

Figures 4c and 4d show the divergence levels of the **exprb43** GPU solver. Similar to the **Radau-IIA** solver, nearly 100 % of warps for the **exprb43** solver have no thread divergence due to differing internal integration step sizes for the hydrogen model. The **exprb43** thread divergence levels increase somewhat for the GRI-Mech 3.0 model with the smaller time-step size; 27 % of warps still had a divergence measure of $D = 0$, but nearly 63 % of the warps had divergence measures between $D = 0.05$ and $D = 0.2$. With the larger time-step size, the **exprb43** solver experiences significantly more thread divergence for both models. The divergence measure distribution is fairly similar to that of the **Radau-IIA** solver for the GRI-Mech 3.0 model, but most warps experience a divergence measure of $D \sim 0.8$ for the hydrogen model (versus $D \sim 0.6$ for the **Radau-IIA** solver). The explicit solvers deal with stiffness less efficiently, and end up using a greater range of internal time-step sizes between conditions of varying stiffness. This results in an increase in thread divergence levels due to differing internal time-step sizes.

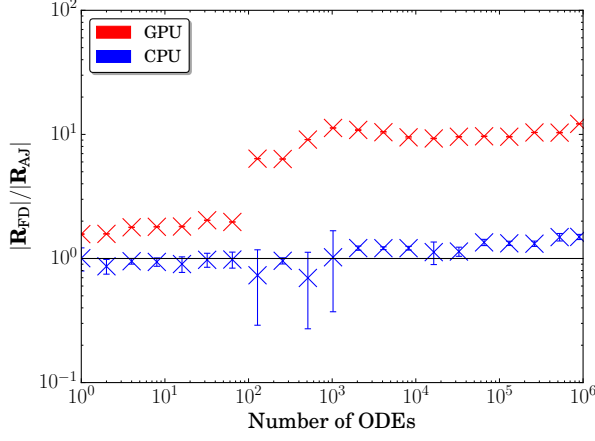
The relatively worse stiffness handling of the **exp4** method is also apparent in Figs. 4e and 4f; in most cases, significantly more thread divergence is seen for **exp4** than for either of the other solvers. The **exp4** algorithm is the only solver to show significant thread divergence even for the hydrogen model for the smaller global time-step size. Further, the **exp4** algorithm experiences more thread divergence than the **exprb43** for both models at the larger global time-step size.

3.4. Effect of using a finite-difference-based chemical kinetic Jacobian

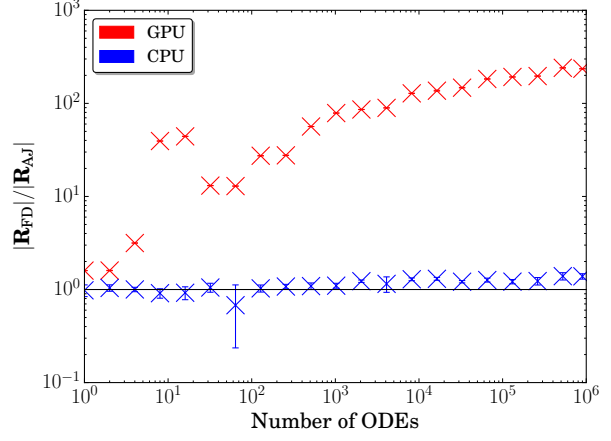
While it is well established that using an analytical Jacobian matrix can significantly accelerate chemical kinetic integration on the CPU (e.g., [5, 58, 61]), relatively little study has been directed at

use of a GPU-based analytical Jacobian. Dijkmans et al. [62] used a GPU-based analytical Jacobian code to accelerate various CPU-based chemical kinetic integration schemes, and our own previous works [30, 31] have detailed the performance of `pyJac`. However, to our knowledge no work using an analytical Jacobian for GPU-based chemical kinetic integration has been published. In this section, we explore the relative performance benefits of the analytical Jacobian compared with a first-order finite-difference Jacobian on both the CPU and GPU. The exponential methods require an exact Jacobian matrix (rather than an approximation as given by finite-difference methods), so their performance was not considered in this section.

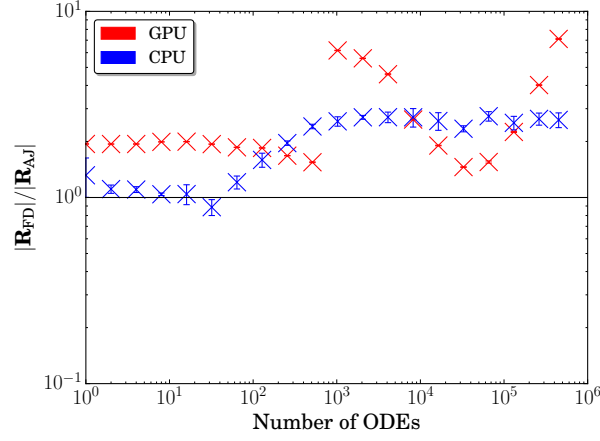
Figure 5 shows the speedup achieved on both the CPU and GPU for the **Radau-IIA** algorithm for various cases; the GRI-Mech 3.0 results for the larger global time-step have been omitted due to long run times. For the hydrogen model (Figs. 5a and 5b), using the analytical Jacobian offers minimal performance benefit for the CPU-based integrators, reaching a maximum speedup of $1.49 \times$ and $1.39 \times$ for the small and large global time-step sizes, respectively. This results from both the relatively small size of the model (and resulting modest chemical source-term evaluation costs), as well as the lower chemical stiffness that requires only a few Jacobian evaluations for the **Radau-IIA** solver. In some cases the finite-difference Jacobian solver may be faster than the analytical Jacobian solver; although it is difficult to explain the exact cause of this phenomena, differences in the finite-difference Jacobian likely caused the integrator to follow a slightly different instruction path (e.g., with fewer Jacobian updates/chemical source term evaluations) changing the integration cost. However, for large numbers of conditions, the analytical-Jacobian-based CPU solver indeed performs faster than the finite-difference counterpart. In contrast, the analytical-Jacobian-based GPU solver performs significantly faster than the finite-difference GPU solver in all cases for the hydrogen model, reaching a maximum speedup of $12.16 \times$ for the smaller global time-step size. As discussed in Sec. 3.3, significantly higher levels of thread divergence are expected for the larger global time-step size. Correspondingly, the maximum speedup of the GPU solver increases to $240.96 \times$ for the larger global time-step size. Figure 5c shows that the speedup of the CPU and GPU solvers reach $2.61 \times$ and $7.11 \times$, respectively, for the larger GRI-Mech 3.0 model at the smaller global time-step size. It is clear that for a per-thread-based GPU integrator, using an analytical Jacobian is essential for efficient integration due to thread-divergence concerns.



(a) Hydrogen model with $\Delta t = 1 \times 10^{-6} \text{ s}$



(b) Hydrogen model with $\Delta t = 1 \times 10^{-4} \text{ s}$



(c) GRI-Mech 3.0 model with $\Delta t = 1 \times 10^{-6} \text{ s}$

Figure 5: Ratio of the average finite-difference Jacobian based integrator runtime $|\mathbf{R}_{\text{FD}}|$ to that of the analytical Jacobian runtime $|\mathbf{R}_{\text{AJ}}|$ for the **Radau-IIA** (CPU/GPU) solvers. Error bars indicate standard deviation, and the horizontal lines show a ratio of one.

4. Conclusions

The large size and chemical stiffness of chemical kinetic models for fuels traditionally requires the use of high-order implicit integrators for efficient solutions. Past work showed orders-of-magnitude speedups for solution of nonstiff to moderately stiff chemical kinetic systems using explicit solvers on GPUs [11, 13, 20]. In contrast, work on stiff chemical kinetic integration with implicit GPU solvers has been limited to specialized cases, or failed to surpass current CPU-based techniques.

This work demonstrated and compared the performances of CPU- and GPU-based integration methods capable of handling greater stiffness, including an implicit fifth-order Runge–Kutta algorithm and two fourth-order exponential integration algorithms, using chemical source term and analytical Jacobian subroutines provided by the pyJac software [29–31]. By comparing the performance of these algorithms using two chemical kinetics models, including hydrogen with 13 species and 54 reactions [43] and methane with 53 species and 325 reactions [44], and using two global time-step sizes (10^{-6} s and 10^{-4} s), we drew the following conclusions:

- For global time-step sizes relevant to large-eddy simulations, the GPU-based implicit Runge–Kutta method was roughly equivalent to the CPU-based implicit `CVODE` integrator running on 12–38 CPU cores.
- At longer global time-step sizes, the performances of all GPU-based integrators decreased significantly due to thread divergence.
- For a global time-step size relevant to Reynolds-averaged Navier–Stokes simulations, the GPU-based implicit Runge–Kutta solver performed equivalent to `CVODE` running on 15 cores for the hydrogen model, and just 3 cores for the GRI-Mech 3.0 model.
- The higher memory traffic required due to the size of the GRI-Mech 3.0 model significantly decreased GPU solver performance; a sparse analytical chemical kinetic Jacobian formulation must be developed to achieve high performance for still larger chemical kinetic models on the GPU.
- The exponential solvers were significantly less efficient than the implicit integrators on the CPU and GPU for all relevant cases.
- Using an analytical Jacobian matrix on the GPU is critical for efficient chemical kinetic integration due to thread divergence; speedups of $7.11\text{--}240.96\times$ over a finite-difference-approximation were reached on the GPU, far surpassing the corresponding CPU speedup of $1.58\text{--}2.61\times$.

Based on these results, we conclude that the exponential solvers poorly fit the SIMD acceleration paradigm due to high levels of thread divergence combined with the relatively high cost of integration steps due to Arnoldi iteration (as compared with other explicit integration techniques). Instead, we recommend directing further focus on stiff explicit solvers such as (non-exponential) Rosenbrock solvers, explored for the CPU by Stone and Bisetti [61], and inexact Jacobian W-methods [63, 64]. Further improvements to the analytical Jacobian code, e.g., by using a chemical kinetic system based on species concentrations to increase Jacobian sparsity, are likely to further increase performance of the developed algorithms. Additionally, newer GPUs should be tested to examine the ability of larger cache sizes and more available registers to improve performance by reduction of slow global memory loads/stores; a per-block solution still may need to be adopted for efficient integration of larger chemical kinetic models. However, this work also showed that thread divergence poses a challenge to high performance of GPU-based integration techniques on a per-thread basis. Our future work will therefore include a more comprehensive study of thread divergence, as well as developing methods to mitigate or eliminate its negative performance impact. Finally, new integration techniques will be investigated and paired with work studying the selection of appropriate solvers based on estimated chemical stiffness.

Acknowledgments

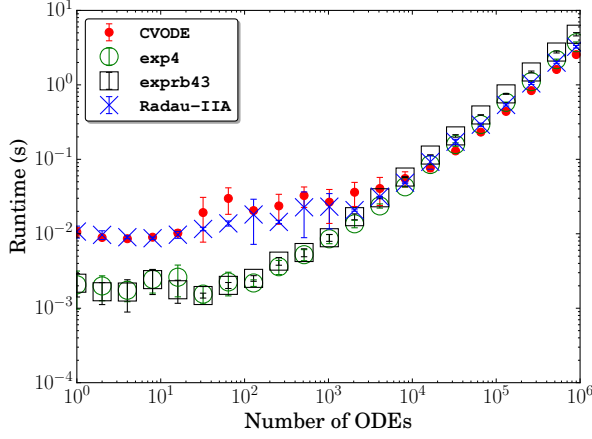
This material is based upon work supported by the National Science Foundation under grants ACI-1534688 and ACI-1535065.

Appendix A. Supplementary material

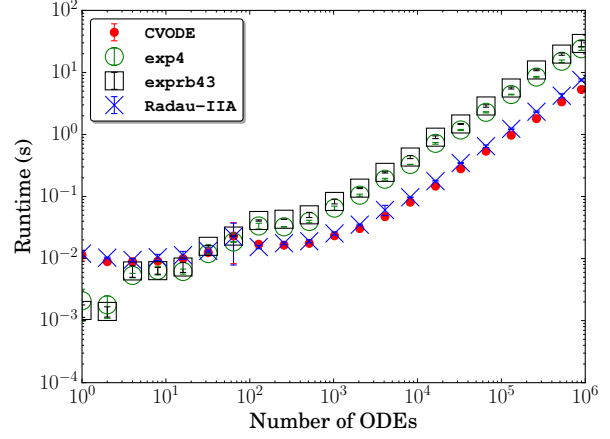
The full L^AT_EX source for this paper is available via a GitHub repository at <https://github.com/arghdos/GPU-Integration-Paper>, including the data and scripts needed to reproduce the figures here.

Appendix B. Raw performance plots

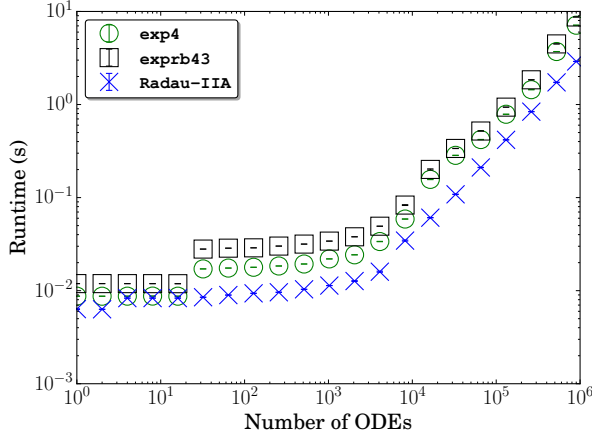
In this section we present the plots of the raw, unnormalized performance data for completeness, as described in Sec. 3. Figures B.1 and B.2 show performance for the hydrogen and GRI-Mech 3.0 models, respectively.



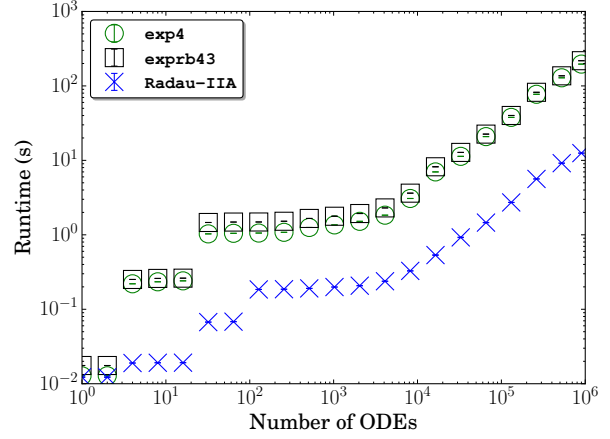
(a) CPU performance results for $\Delta t = 10^{-6}$ s



(b) CPU performance results for $\Delta t = 10^{-4}$ s

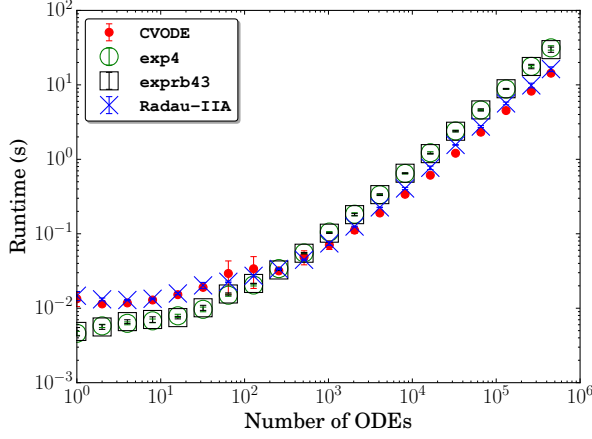


(c) GPU performance results for $\Delta t = 10^{-6}$ s

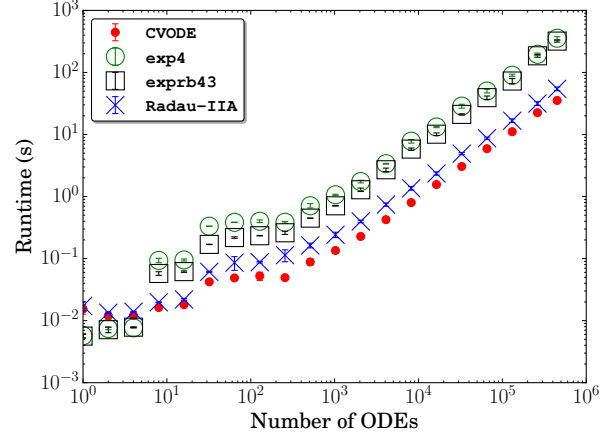


(d) GPU performance results for $\Delta t = 10^{-4}$ s

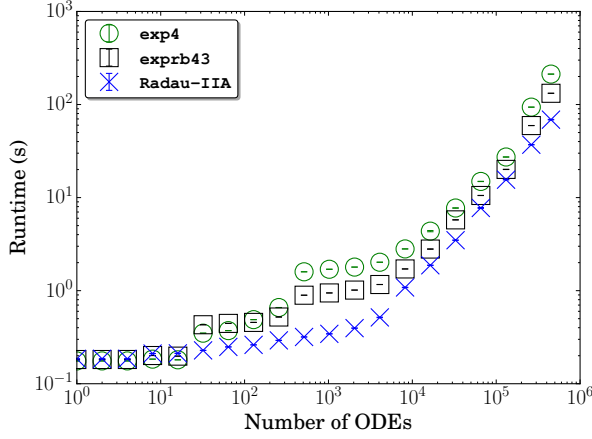
Figure B.1: Average (unnormalized) runtimes of the integrators on the CPU and GPU for the hydrogen model at two different global time-step sizes. Error bars indicate standard deviation.



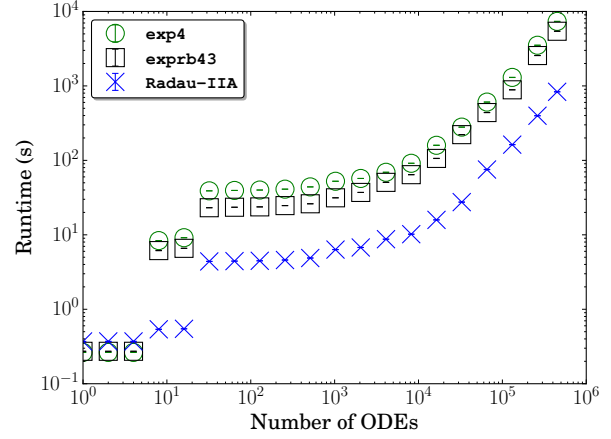
(a) CPU performance results for $\Delta t = 10^{-6}$ s



(b) CPU performance results for $\Delta t = 10^{-4}$ s



(c) GPU performance results for $\Delta t = 10^{-6}$ s



(d) GPU performance results for $\Delta t = 10^{-4}$ s

Figure B.2: Average (unnormalized) runtimes of the integrators on the CPU/GPU for the GRI-Mech 3.0 model at two different global time-step sizes. Error bars indicate standard deviation.

References

- [1] C. V. Naik, K. V. Puduppakkam, A. Modak, E. Meeks, Y. L. Wang, Q. Feng, T. T. Tsotsis, Detailed chemical kinetic mechanism for surrogates of alternative jet fuels, *Combust. Flame* 158 (3) (2011) 434–445. [doi:10.1016/j.combustflame.2010.09.016](https://doi.org/10.1016/j.combustflame.2010.09.016).
- [2] S. M. Sarathy, C. K. Westbrook, M. Mehl, W. J. Pitz, C. Togbe, P. Dagaut, H. Wang, M. A. Oehlschlaeger, U. Niemann, K. Seshadri, P. S. Veloo, C. Ji, F. N. Egolfopoulos, T. Lu, Comprehensive chemical kinetic modeling of the oxidation of 2-methylalkanes from C₇ to C₂₀, *Combust. Flame* 158 (12) (2011) 2338–2357. [doi:10.1016/j.combustflame.2011.05.007](https://doi.org/10.1016/j.combustflame.2011.05.007).
- [3] M. Mehl, J.-Y. Chen, W. J. Pitz, S. M. Sarathy, C. K. Westbrook, An approach for formulating surrogates for gasoline with application toward a reduced surrogate mechanism for CFD engine modeling, *Energy Fuels* 25 (11) (2011) 5215–5223. [doi:10.1021/ef201099y](https://doi.org/10.1021/ef201099y).
- [4] O. Herbinet, W. J. Pitz, C. K. Westbrook, Detailed chemical kinetic mechanism for the oxidation of biodiesel fuels blend surrogate, *Combust. Flame* 157 (5) (2010) 893–908. [doi:10.1016/j.combustflame.2009.10.013](https://doi.org/10.1016/j.combustflame.2009.10.013).
- [5] T. Lu, C. K. Law, Toward accommodating realistic fuel chemistry in large-scale computations, *Prog. Energy Comb. Sci.* 35 (2) (2009) 192–215. [doi:10.1016/j.pecs.2008.10.002](https://doi.org/10.1016/j.pecs.2008.10.002).
- [6] J. Nickolls, I. Buck, M. Garland, K. Skadron, Scalable parallel programming with CUDA, *ACM Queue* 6 (2) (2008) 40–53. [doi:10.1145/1365490.1365500](https://doi.org/10.1145/1365490.1365500).
- [7] NVIDIA, CUDA C programming guide, version 7.5, https://docs.nvidia.com/cuda/pdf/CUDA_C_Programming_Guide.pdf (Sep. 2015).
- [8] F. A. Cruz, S. K. Layton, L. A. Barba, How to obtain efficient GPU kernels: An illustration using FMM & FGT algorithms, *Comput. Phys. Comm.* 182 (10) (2011) 2084–2098. [doi:10.1016/j.cpc.2011.05.002](https://doi.org/10.1016/j.cpc.2011.05.002).
- [9] A. R. Brodtkorb, T. R. Hagen, M. L. Sætra, Graphics processing unit (GPU) programming strategies and trends in GPU computing, *J. Parallel Distrib. Comput.* 73 (1) (2013) 4–13. [doi:10.1016/j.jpdc.2012.04.003](https://doi.org/10.1016/j.jpdc.2012.04.003).

- [10] K. E. Niemeyer, C. J. Sung, Recent progress and challenges in exploiting graphics processors in computational fluid dynamics, *J. Supercomput.* 67 (2) (2014) 528–564. [doi:10.1007/s11227-013-1015-7](https://doi.org/10.1007/s11227-013-1015-7).
- [11] K. E. Niemeyer, C. J. Sung, C. G. Fotache, J. C. Lee, Turbulence-chemistry closure method using graphics processing units: a preliminary test, in: Fall 2011 Technical Meeting of the Eastern States Section of the Combustion Institute. [doi:10.6084/m9.figshare.3384964](https://doi.org/10.6084/m9.figshare.3384964).
- [12] C. P. Stone, R. L. Davis, Techniques for solving stiff chemical kinetics on graphical processing units, *J. Propul. Power* 29 (4) (2013) 764–773. [doi:10.2514/1.B34874](https://doi.org/10.2514/1.B34874).
- [13] K. E. Niemeyer, C. J. Sung, Accelerating moderately stiff chemical kinetics in reactive-flow simulations using GPUs, *J. Comput. Phys.* 256 (2014) 854–871. [doi:10.1016/j.jcp.2013.09.025](https://doi.org/10.1016/j.jcp.2013.09.025).
- [14] F. Sewerin, S. Rigopoulos, A methodology for the integration of stiff chemical kinetics on GPUs, *Combust. Flame* 162 (4) (2015) 1375–1394. [doi:10.1016/j.combustflame.2014.11.003](https://doi.org/10.1016/j.combustflame.2014.11.003).
- [15] K. Spafford, J. Meredith, J. Vetter, J. Chen, R. Grout, R. Sankaran, Accelerating S3D: A GPGPU case study, in: Euro-Par 2009 Parallel Processing Workshops, LNCS 6043, Springer-Verlag, Berlin, Heidelberg, 2010, pp. 122–131. [doi:10.1007/978-3-642-14122-5_16](https://doi.org/10.1007/978-3-642-14122-5_16).
- [16] Y. Shi, W. H. Green, H.-W. Wong, O. O. Oluwole, Redesigning combustion modeling algorithms for the graphics processing unit (GPU): Chemical kinetic rate evaluation and ordinary differential equation integration, *Combust. Flame* 158 (5) (2011) 836–847. [doi:10.1016/j.combustflame.2011.01.024](https://doi.org/10.1016/j.combustflame.2011.01.024).
- [17] R. J. Kee, F. M. Rupley, J. A. Miller, Chemkin-II: A Fortran chemical kinetics package for the analysis of gas-phase chemical kinetics, Tech. rep., Sandia National Labs., Livermore, CA (1989).
- [18] E. Anderson, Z. Bai, C. Bischof, S. Blackford, J. Demmel, J. Dongarra, J. Du Croz, A. Greenbaum, S. Hammarling, A. McKenney, D. Sorensen, LAPACK Users’ Guide, 3rd Edition, SIAM, Philadelphia, PA, 1999.
- [19] Y. Shi, W. H. Green, H.-W. Wong, O. O. Oluwole, Accelerating multi-dimensional combustion simulations using GPU and hybrid explicit/implicit ODE integration, *Combust. Flame* 159 (7) (2012) 2388–2397. [doi:10.1016/j.combustflame.2012.02.016](https://doi.org/10.1016/j.combustflame.2012.02.016).

- [20] H. P. Le, J.-L. Cambier, L. K. Cole, GPU-based flow simulation with detailed chemical kinetics, *Comput. Phys. Comm.* 184 (3) (2013) 596–606. [doi:10.1016/j.cpc.2012.10.013](https://doi.org/10.1016/j.cpc.2012.10.013).
- [21] P. N. Brown, G. D. Byrne, A. C. Hindmarsh, VODE: a variable-coefficient ODE solver, *SIAM J. Sci. Stat. Comput.* 10 (5) (1989) 1038–1051. [doi:10.1137/0910062](https://doi.org/10.1137/0910062).
- [22] G. Wanner, E. Hairer, *Solving ordinary differential equations II*, 2nd Edition, Springer-Verlag, Berlin, 1996. [doi:10.1007/978-3-642-05221-7](https://doi.org/10.1007/978-3-642-05221-7).
- [23] A. C. Hindmarsh, P. N. Brown, K. E. Grant, S. L. Lee, R. Serban, D. E. Shumaker, C. S. Woodward, SUNDIALS: Suite of nonlinear and differential/algebraic equation solvers, *ACM T. Math. Softw.* 31 (3) (2005) 363–396. [doi:10.1145/1089014.1089020](https://doi.org/10.1145/1089014.1089020).
- [24] F. Perini, E. Galligani, R. D. Reitz, A study of direct and Krylov iterative sparse solver techniques to approach linear scaling of the integration of chemical kinetics with detailed combustion mechanisms, *Combust. Flame* 161 (5) (2014) 1180–1195. [doi:10.1016/j.combustflame.2013.11.017](https://doi.org/10.1016/j.combustflame.2013.11.017).
- [25] M. J. McNenly, R. A. Whitesides, D. L. Flowers, Faster solvers for large kinetic mechanisms using adaptive preconditioners, *Proc. Combust. Inst.* 35 (1) (2015) 581–587. [doi:10.1016/j.proci.2014.05.113](https://doi.org/10.1016/j.proci.2014.05.113).
- [26] M. Hochbruck, C. Lubich, On Krylov subspace approximations to the matrix exponential operator, *SIAM J. Numer. Anal.* 34 (5) (1997) 1911–1925. [doi:10.1137/S0036142995280572](https://doi.org/10.1137/S0036142995280572).
- [27] F. Bisetti, Integration of large chemical kinetic mechanisms via exponential methods with Krylov approximations to Jacobian matrix functions, *Combust. Theor. Model.* 16 (3) (2012) 387–418. [doi:10.1080/13647830.2011.631032](https://doi.org/10.1080/13647830.2011.631032).
- [28] M. Falati, G. Hojjati, Integration of chemical stiff odes using exponential propagation method, *J. Math. Chem.* 49 (10) (2011) 2210–2230. [doi:10.1007/s10910-011-9881-9](https://doi.org/10.1007/s10910-011-9881-9).
- [29] K. E. Niemeyer, N. J. Curtis, *pyJac v1.0.1* (May 2016). [doi:10.5281/zenodo.53100](https://doi.org/10.5281/zenodo.53100).
- [30] K. E. Niemeyer, N. J. Curtis, C. J. Sung, Initial investigation of *pyJac*: an analytical jacobian generator for chemical kinetics, in: *Fall 2015 Meeting of the West. States Sect. Combust. Inst.*, 2015. [doi:10.6084/m9.figshare.2075515](https://doi.org/10.6084/m9.figshare.2075515).

- [31] K. E. Niemeyer, N. J. Curtis, C. J. Sung, pyJac: analytical Jacobian generator for chemical kinetics, under review. [arXiv:1605.03262](https://arxiv.org/abs/1605.03262) [physics.comp-ph] (May 2016).
- [32] A. C. Hindmarsh, R. Serban, CVODE v2.8.2, <http://computation.llnl.gov/projects/sundials-suite-nonlinear-differential-algebraic-equation-solvers/download/cvode-2.8.2.tar.gz> (Aug. 2015).
- [33] E. Banks, A. M. Collier, A. C. Hindmarsh, R. Serban, C. S. Woodward, SUNDIALS v2.6.2, <http://computation.llnl.gov/projects/sundials-suite-nonlinear-differential-algebraic-equation-solvers/download/sundials-2.6.2.tar.gz> (Aug. 2015).
- [34] M. Hochbruck, C. Lubich, H. Selhofer, Exponential integrators for large systems of differential equations, SIAM J. Sci. Comput. 19 (5) (1998) 1552–1574. [doi:10.1137/S1064827595295337](https://doi.org/10.1137/S1064827595295337).
- [35] M. Hochbruck, A. Ostermann, J. Schweitzer, Exponential Rosenbrock-type methods, SIAM J. Numer. Anal. 47 (1) (2009) 786–803. [doi:10.1137/080717717](https://doi.org/10.1137/080717717).
- [36] E. Gallopoulos, Y. Saad, Efficient solution of parabolic equations by Krylov approximation methods, SIAM J. Sci. Stat. Comp. 13 (5) (1992) 1236–1264. [doi:10.1137/0913071](https://doi.org/10.1137/0913071).
- [37] L. N. Trefethen, J. A. C. Weideman, T. Schmelzer, Talbot quadratures and rational approximations, BIT Numer. Math. 46 (3) (2006) 653–670. [doi:10.1007/s10543-006-0077-9](https://doi.org/10.1007/s10543-006-0077-9).
- [38] K. E. Niemeyer, cf_expm v1.0 (Jan. 2016). [doi:10.5281/zenodo.44291](https://doi.org/10.5281/zenodo.44291).
- [39] M. Frigo, S. G. Johnson, The design and implementation of FFTW3, Proc. IEEE 93 (2) (2005) 216–231. [doi:10.1109/JPROC.2004.840301](https://doi.org/10.1109/JPROC.2004.840301).
- [40] M. Frigo, S. G. Johnson, FFTW v3.3.4, <http://www.fftw.org/> (Mar. 2014).
- [41] G. W. Stewart, Matrix Algorithms: Volume 1: Basic Decompositions, SIAM, Philadelphia, 1998. [doi:10.1137/1.9781611971408](https://doi.org/10.1137/1.9781611971408).
- [42] Y. Saad, Analysis of some Krylov subspace approximations to the matrix exponential operator, SIAM J. on Numer. Anal. 29 (1) (1992) 209–228. [doi:10.1137/0729014](https://doi.org/10.1137/0729014).
- [43] M. P. Burke, M. Chaos, Y. Ju, F. L. Dryer, S. J. Klippenstein, Comprehensive H₂/O₂ kinetic model for high-pressure combustion, Int. J. Chem. Kinet. 44 (7) (2011) 444–474. [doi:10.1002/kin.20603](https://doi.org/10.1002/kin.20603).

- [44] G. P. Smith, D. M. Golden, M. Frenklach, N. W. Moriarty, B. Eiteneer, M. Goldenberg, C. T. Bowman, R. K. Hanson, S. Song, W. C. Gardiner, V. V. Lissianski, Z. Qin, GRI-Mech 3.0, http://www.me.berkeley.edu/gri_mech/ (1999).
- [45] J.-Y. Chen, Stochastic modeling of partially stirred reactors, *Combust. Sci. Technol.* 122 (1–6) (1997) 63–94. doi:[10.1080/00102209708935605](https://doi.org/10.1080/00102209708935605).
- [46] S. B. Pope, Computationally efficient implementation of combustion chemistry using in situ adaptive tabulation, *Combust. Theor. Model.* 1 (1) (1997) 41–63. doi:[10.1080/713665229](https://doi.org/10.1080/713665229).
- [47] Z. Ren, Y. Liu, T. Lu, L. Lu, O. O. Oluwole, G. M. Goldin, The use of dynamic adaptive chemistry and tabulation in reactive flow simulations, *Combust. Flame* 161 (1) (2014) 127–137. doi:[10.1016/j.combustflame.2013.08.018](https://doi.org/10.1016/j.combustflame.2013.08.018).
- [48] B. N. Datta, *Numerical Linear Algebra and Applications*, SIAM, Philadelphia, PA, 2010.
- [49] M. Hochbruck, A. Ostermann, Exponential integrators, *Acta Numer.* 19 (2010) 209–286. doi:[10.1017/S0962492910000048](https://doi.org/10.1017/S0962492910000048).
- [50] H. Yang, Z. Ren, T. Lu, G. M. Goldin, Dynamic adaptive chemistry for turbulent flame simulations, *Combust. Theor. Model.* 17 (1) (2013) 167–183.
- [51] G. Iaccarino, A. Ooi, P. Durbin, M. Behnia, Reynolds averaged simulation of unsteady separated flow, *Int. J. Heat Fluid Flow* 24 (2) (2003) 147–156. doi:[10.1016/S0142-727X\(02\)00210-2](https://doi.org/10.1016/S0142-727X(02)00210-2).
- [52] H. Wang, S. B. Pope, Large eddy simulation/probability density function modeling of a turbulent jet flame, *Proc. Combust. Inst.* 33 (1) (2011) 1319–1330. doi:[10.1016/j.proci.2010.08.004](https://doi.org/10.1016/j.proci.2010.08.004).
- [53] G. Bulat, W. P. Jones, A. J. Marquis, Large eddy simulation of an industrial gas-turbine combustion chamber using the sub-grid PDF method, *Proc. Combust. Inst.* 34 (2) (2013) 3155–3164. doi:[10.1016/j.proci.2012.07.031](https://doi.org/10.1016/j.proci.2012.07.031).
- [54] J. A. Ramírez, C. Cortés, Comparison of different URANS schemes for the simulation of complex swirling flows, *Numer. Heat Transf., Part B: Fundam.* 58 (2) (2010) 98–120. doi:[10.1080/10407790.2010.508440](https://doi.org/10.1080/10407790.2010.508440).

- [55] E. Galloni, Analyses about parameters that affect cyclic variation in a spark ignition engine, *Applied Thermal Engineering* 29 (5–6) (2009) 1131–1137. doi:[10.1016/j.applthermaleng.2008.06.001](https://doi.org/10.1016/j.applthermaleng.2008.06.001).
- [56] Intel, Intel® Xeon® Processor E5-4640 v2 (20M Cache, 2.20 GHz), http://ark.intel.com/products/75288/Intel-Xeon-Processor-E5-4640-v2-20M-Cache-2_20-GHz, accessed: 06-06-2016.
- [57] Amazon.com, Buying Choices: NVIDIA Tesla C2075 6GB GDDR5 PCIe Workstation Card, http://www.amazon.com/gp/offer-listing/B0050CMZ7A/ref=dp_olp_all_mbc?ie=UTF8&condition=all, accessed: 06-06-2016.
- [58] D. A. Schwer, J. E. Tolsma, W. H. Green, P. I. Barton, On upgrading the numerics in combustion chemistry codes, *Combust. Flame* 128 (3) (2002) 270–291. doi:[10.1016/S0010-2180\(01\)00352-2](https://doi.org/10.1016/S0010-2180(01)00352-2).
- [59] Amazon.com, Tesla K40 Graphic Card - 1 GPUs - 745 MHz Core - 12 GB GDDR5 SDRAM , <https://www.amazon.com/Tesla-K40-Graphic-Card-GDDR5/dp/B00KDRRTB8>, accessed: 07-07-2016.
- [60] NVIDIA, NVIDIA Tesla GPUs Datasheet, <http://docs.nvidia.com/cuda/cuda-c-programming-guide/index.html#compute-capabilities>, accessed: 07-07-2016.
- [61] C. P. Stone, F. Bisetti, Comparison of ODE solvers for chemical kinetics and reactive CFD applications, in: *AIAA 52nd Aerospace Sciences Meeting* (National Harbor, MD), 2014. doi:[10.2514/6.2014-0822](https://doi.org/10.2514/6.2014-0822).
- [62] T. Dijkmans, C. M. Schietekat, K. M. Van Geem, G. B. Marin, GPU based simulation of reactive mixtures with detailed chemistry in combination with tabulation and an analytical Jacobian, *Comput. Chem. Eng.* 71 (2014) 521–531. doi:[10.1016/j.compchemeng.2014.09.016](https://doi.org/10.1016/j.compchemeng.2014.09.016).
- [63] T. Steihaug, A. Wolfbrandt, An attempt to avoid exact jacobian and nonlinear equations in the numerical solution of stiff differential equations, *Math. of Comput.* 33 (146) (1979) 521–534.
- [64] B. A. Schmitt, R. Weiner, Parallel two-step w-methods with peer variables, *SIAM J. on Numer. Anal.* 42 (1) (2004) 265–282. doi:[10.1137/S0036142902411057](https://doi.org/10.1137/S0036142902411057).